High-resolution spatial analysis of a hurricane structure by means of X-band and Ka-band satellite synthetic aperture radar

Saverio Mori[1,2], Federica Polverari[1,2], Luca Pulvirenti[3], Mario Montopoli[1,2], Nazzareno Pierdicca[1] and Frank Silvio Marzano[1,2]

[1]*DIET University of Rome, Italy*
[2]*CETEMPS, University of L'Aquila, Italy*
[3]*CIMA, Savona, Italy*

Saverio Mori

(Dated: 21 July 2014)

1 Introduction

Spaceborne synthetic aperture radars (SARs) have very good spatial resolution (of the order of hundreds meters in presence of precipitations) and the capability of fully characterize the extinction and scattering properties of the target. Nowadays several spaceborne SAR systems are operational, such as the Cosmo-SkyMed constellation (Covello et al., 2010) and TerraSAR-X/TanDEM-X (Werninghaus et al., 2010), ensuring a great ground coverage, but also increasing the probability of observing precipitation events. Moreover, several projects are currently analyzing the feasibility of spaceborne SAR systems operating at higher frequency, such as Ka-band. So far, several sensitivity studies of SAR amplitude and phase received signal to atmospheric effects, and in particular to precipitations , have been assessed for frequencies above C band by numerous investigators in the last years, e.g. (Danklmayer et al., 2009), (Marzano et al., 2011), (Baldini et al., 2014).

In particular SAR systems operating at X-Band have proved to be sensitive to intense precipitation events, such as hurricanes, tropical storms (e.g., Marzano et al., 2010) or mid-latitude heavy rainfalls (e.g., Pulvirenti et al., 2014). The sensitivity of higher frequency SARs to intense atmospheric precipitations represents an attractive possibility to have new insights on these events (e.g. (Marzano et al., 2012)). From a theoretical perspective, the impact of precipitation on SAR slant-viewing imagery is due to the combination of surface and volumetric backscattering, coupled with path attenuation. Both scattering and path attenuation effects are expected to have a significant dependence on frequency, polarization and spatial distribution of hydrometeors. Nevertheless, several aspects of the interaction between the SARs response and rain precipitations require a deeper insight. In this respect a valid aid is the analysis of simulated atmospheric scenarios coupled with a suitable electromagnetic model.

In previous works we developed a model of spaceborne SAR response to several ground targets in presence of precipitating cloud systems (Marzano et al., 2012). This model allowed simulating 2-D (two-dimensional) volume scenarios (terrain and atmosphere) derived by realistic mesoscale meteorological models, with hydrometeors distribution generated by mean of a high resolution cloud resolving model, hydrometeors electromagnetic characterization given by HESS (Hydrometeor Ensemble Scattering Simulator) T-Matrix simulations, and ground target scattering described by semi-empirical models. The model, used in this work for simulating the SAR response is an evolution of the simplified one proposed in (Weinman and Marzano, 2008) where cloud systems were characterized by rain and snow 2-D distributions factorized by means of *ad hoc* analytical functions.

In this work we have revised the model framework, better characterizing the signal amplitude response and giving a more complete model of the signal differential phase shift. The latter is expressed in terms of the complex correlation coefficient and includes the incoherent summation of surface and volume contributions. Moreover, we have extended the ground target model to include sea surfaces and bare soils terrain targets. Description of the SAR response model framework is given in section 2. Section 3 shows a comparison with the previous version of the model, and examples of simulations for both X and Ka bands, assuming bare soil and marine surface as background. Conclusions are drawn in section 4.

2 SARs response forward model

The high-spatial resolution of SAR observations gives the opportunity to resolve cloud convection and turbulence at their proper scales. For this reason it is important generating synthetic scenarios able to catch such scales and then give information on the expected SAR signal when the ray path intercept atmospheric precipitation. The System for Atmospheric Modeling (SAM), described in the sequel, well suited for the aforementioned purpose (e.g. Marzano et al., 2012).

Realistic simulations of SAR observations of precipitation require modeling the surface contribution. In this work we have considered both a bare soil surface and a marine one which are modelled by the Semi Empirical Model proposed by Oh et al. (2002) (hereafter denoted as SEM) and the SEAWIND2 model (Pierdicca and Pulvirenti, 2008), respectively. As for the atmospheric contribution, the outputs of the HESS T-Matrix model that describes the interaction of the electromagnetic signal with hydrometeors have been incorporated into the simulations.

2.1 SAR Polarimetric Observables

A fully polarimetric SAR system can measure three backscattering complex components, expressed in vector form as $\boldsymbol{\Omega}_{SAR}=[S_{SARhh}\ \sqrt{2}S_{SARhv}\ S_{SARvv}]^T$, where S_{SARpq} are the elements of the backscattering complex matrix $\boldsymbol{S}_{SAR}$, the subscripts p and q represent the radar receive and transmit linear (horizontal h or vertical v) polarizations, respectively, and reciprocity is assumed (e.g., (Bringi 2001), (Ulaby 1990)). The subscript "SAR" is intended to discriminate between the surface backscattering, represented by a complex vector $\boldsymbol{\Omega}=[S_{hh}\ \sqrt{2}S_{hv}\ S_{vv}]^T$, and the spaceborne measured quantities, affected by the propagation through the atmosphere from the surface to the SAR antenna. In this respect we have considered the post processed SAR as equivalent to a side-looking real aperture radar (SLAR). The equivalence of SARs observing precipitations with SLARs is analyzed in (Marzano et al., 2012). Briefly, when SARs observe precipitations, their high resolution (order of meters) data are degraded to a lower value (about 500 m/pixel at X-Band), which approach the one of a SLAR systems.

The medium propagation effects may be described by the forward-scattering matrix $\boldsymbol{F}$ (which is the complex scattering matrix computed in the forward direction). The resulting 3×3 ensemble-average scattering covariance matrix $\boldsymbol{C}_{SAR}=<\boldsymbol{\Omega}_{SAR}\boldsymbol{\Omega}_{SAR}{}^{*T}>$ is the SAR-measured polarimetric covariance which contains the relationships among the radar backscattering observations, including the propagation effects (Ulaby, 1990). Note that the angle brackets represent the ensemble average operator over space–time realizations of the observed scene and that the quantities are normalized to the ground projected area. Finally, we can define the following SAR polarimetric observables (Bringi, 2001; Ulaby, 1990):

$$\begin{aligned}\sigma^0{}_{SARppqq}(x,y)&=(4\pi/A)<S_{SARpp}(x,y)S_{SARqq}{}^*(x,y)>\\ \sigma^0{}_{SARpq}(x,y)&=(4\pi/A)<S_{SARpq}(x,y)S_{SARpq}{}^*(x,y)>\end{aligned} \tag{2.1}$$

$$\rho_{SARco}(x,y)=\frac{<S_{SARhh}(x,y)S_{SARvv}{}^*(x,y)>}{\sqrt{<|S_{SARhh}(x,y)|^2>}\sqrt{<|S_{SARvv}(x,y)|^2>}}=|\rho_{SARco}(x,y)|e^{j\Psi_{SARco}(x,y)} \tag{2.2}$$

In (2.1) $\sigma^0{}_{SARpppp}$ and $\sigma^0{}_{SARpq}$ are the well-known co-polarized and cross-polarized Normalized Radar Cross Sections (NRCS, adimensional), otherwise denotes as $\sigma^o{}_{SARvv}$, $\sigma^o{}_{SARhh}$, and $\sigma^o{}_{SARhv}$, but we have distinguished the product of the cross-polar S_{SARpq} and co-polar S_{SARpp}, S_{SARqq} scattering coefficients to extend the definition to all the terms of the polarimetric covariance matrix. In (2.2) ρ_{SARco} is the complex correlation coefficient (adimensional) whose argument is $\psi_{SARco.}$ The pixel coordinates are x, y while A is the pixel area.

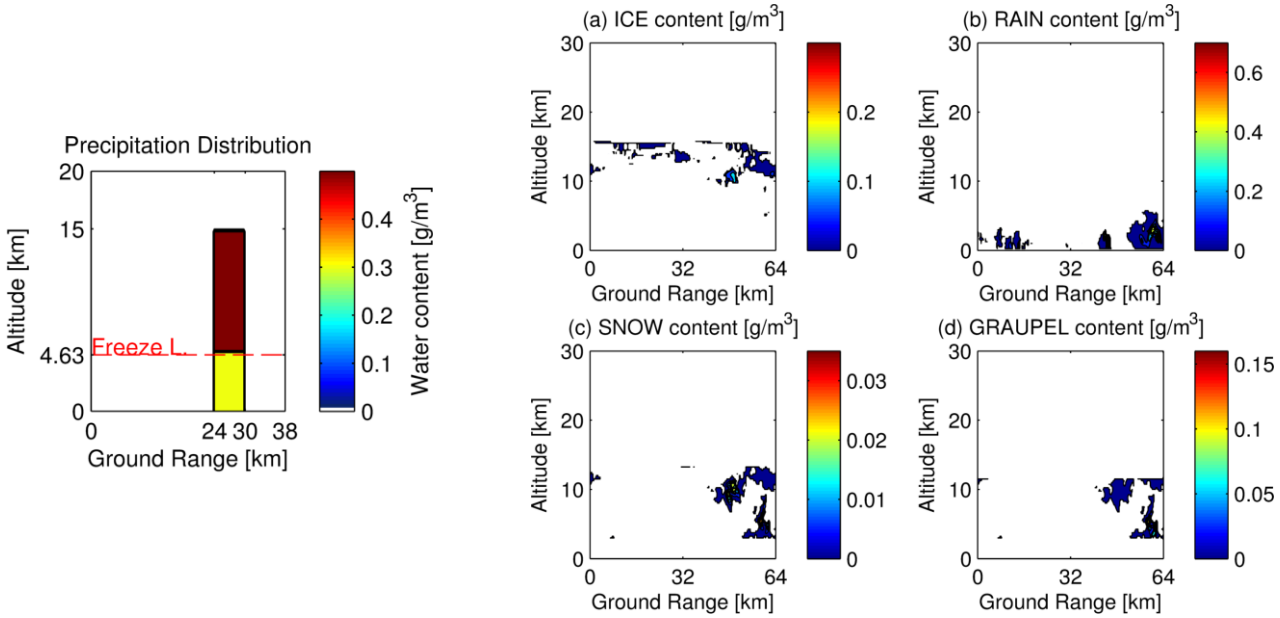

Fig. 1. Hydrometeor water content [g/m^3] distributions for the two test cases considered in this work. (Left) Basic test case, where the precipitating cloud is described by a rectangular homogeneous distribution of rain (up to freezing level) and snow (above) particles.(Right) Distribution of ice, rain, snow and graupel particles in a vertical (x-z plane) section of a SAM Kwajex simulation.

2.2 Atmospheric scenarios simulations

In this work we have simulated the atmospheric hydrometeor distributions by mean of two different models. The first one, based on the one described in (Weinman and Marzano, 2008), and adopted for testing purposes, is characterized by two

layers of liquid water and frozen hydrometeors. For sake of simplicity we have considered a rectangular shape for the particles distribution, while hydrometeors are model by mean of their water content [g/m^3], more suitable to represent both frozen and liquid particles. Obviously this kind of model is unrealistic but it is useful to understand, at first instance, the SAR response in presence of precipitations. In this work we have implemented the simplified model of Weinman and Marzano et al., 2012 to verify our suggested upgrades.

A more realistic atmospheric simulator is the System for Atmospheric Model (SAM), an advanced cloud-resolving model (CRM) particularly suited for high-resolution microphysical studies. SAM can simulate 3-D distribution of hydrometeors, both precipitating (rain, snow, graupel) and non-precipitating (cloud ice and cloud liquid water), expressed by their water content. In this work we have used a dataset generated using SAM 6.3 for the Kwajalein Experiment (KWAJEX), relative to Julian date 207.04 and 208.58, 1999 (Blossey et al., 2007). The dataset consists of volumes of 64 x 64 km^2 and 30 km height, ground resolution of 250 m and varying vertical resolution, ranging from less than 250 m up to 3 km height, and until 800 m near 30 km height. Dataset dimensions and resolution are comparable with those achievable from spaceborne SAR observing a turbulent medium. The dataset was generated for an oceanic scenario: in this preliminary work we have superimposed SAM cloud structures both to a bare soil and to a sea surface, assumed horizontally uniform, in order to investigate atmospheric signatures in presence of realistic surface backgrounds. For this preliminary work we have chosen a vertical section of hydrometeors (on *x-z* plane), among those available in SAM, neither too "dense" nor too "light", representing a "medium" scenery. Figure 1 shows the two test cases adopted for this work.

2.3 Ground surface scenarios simulations

In this work we have considered two kinds of earth surfaces, a bare soil one and a sea surface one. Bare soil is modelled by the Semi Empirical Model (SEM) described in (Oh et al., 2002), which allows expressing not only the amplitude, but also the phase difference of the backscattered SAR response by mean of the degree of correlation $|\rho_{co}|$ and co-polarized differential phase δ_{co}:

$$\rho_{co}^{ground} = \left|\rho_{co}^{ground}\right| e^{j\delta_{co}^{ground}} \tag{2.3}$$

The SEM input parameters are the incident angle θ (radians), the wavenumber k (adimensional), the volumetric soil moisture content m_v of the top 3 cm of soil surface (cm^3·cm^{-3}), the terrain roughness correlation length l (cm), and the root-mean-square (rms) height s (cm): in this work we have considered $l = 5.0$ *cm*, $s = 1.5$ cm and $m_v = 0.25$, within the expected ranges indicated in Oh et al. (2002) and corresponding to a background NRCS of about -6 dB for $\theta = 35$ (deg) and $f = 9.6$ GHz. To better analyze the atmospheric SAR response, we have extended the derived value on the entire scene, simulating a near uniform bare soil surface.

Sea surfaces have been simulated by mean of the SEAWIND2 model described in (Pierdicca and Pulvirenti, 2008), for the same wavelength and incident angle. The SEAWIND2 software provides numerical simulations of both brightness temperature (T_B) and the backscattering coefficient (σ^0) of the sea surface at any frequency, within a unified approach based on the two-scale model of the sea surface. This method assumes the sea surface as composed by two scales of roughness, tha is small-scale gravity-capillary waves which are superimposed on large-scale gravity waves. The considered sea surface spectrum is valid for a fully developed sea and it depends on the friction velocity $u*(v_w,z)$ (m/s), that can be expressed through the wind speed v_w (m/s) at height z (m) AMSL. Table I shows same example of σ^0_{hh}, σ^0_{vv} (dB) for different wind speed at 10 m AMSL.

Table 1:SEAWIND2 σ^0_{hh}, σ^0_{vv} at 10 m a.s.l for different wind speed (m/s).

	1 m/s	5 m/s	10 m/s	15 m/s	20 m/s
σ^0_{hh} (dB)	-37.64	.21.67	-16.27	-13.63	-11.77
σ^0_{vv} (dB)	-32.71	-17.38	-12.47	-10.10	-8.43

SAM KWAJEX simulations include wind speed 3-D components for each surface points and heights. In this preliminary work we have considered wind speed at 23.7 m for a given x-z slice to derive the polarimetric signature of a sea surface using SEAWIND2. Unfortunately SEAWIND2 does not allow simulating the complex correlation coefficient.

2.4 Polarimetric SAR response simulation

In presence of precipitation the SAR backscattering response has to account for the two-way attenuation of surface echoes due to precipitations, the atmospheric volume reflectivity and phase shift. With x and y we indicate the cross-track and along-track ground coordinates, respectively, whereas the altitude is indicated by z. For a given pixel (x,y), the spaceborne SAR co-polar (*pp* or *qq*) and cross-polar (*pq*) NRCS can be formally expressed by (e.g., Weinman and Marzano, 2008):

$$\sigma_{SARpq}(x,y) = \sigma_{SRFpq}(x,y) + \sigma_{VOLpq}(x,y) \tag{2.4}$$

where $\sigma_{SRFpq}(x,y)$ and $\sigma_{VOLpq}(x,y)$ ($m^{2}\cdot m^{-2}$) are respectively the "surface-driven" and "volume-driven" backscattering, the first accounting for the ground surface response and the second for the atmospheric contribution by means of hydrometeors reflectivity. Both surface and volume terms are weighted by the two way path attenuation. In this respect we have revised the model described in (Marzano et al., 2012) by clearly specifying the forward and backward contributions to the differential two-way extinction:

$$L(x,y) = \exp\left(- \int_{\Delta l(x,y)} k_{qq}(l)dl - \int_{\Delta l(x,y)} k_{pp}(l)dl \right) \tag{2.5}$$

where $k_{xx}(l)$ is the co-polar (at polarization x) specific attenuation (1/km) of hydrometeors, while l (km) is the coordinate along the signal path (see Figure 2) and $L(x,y)$ represents differential path attenuation at coordinates x,y. In this work we have revised also the complex correlation coefficient whose final expression is:

$$\rho_{\mathrm{SARco}} = \frac{f\left(\sigma_{hh}^{ground}, \sigma_{vv}^{ground}, \rho_{co}^{ground}\right) \cdot L\left(k_{hh}, k_{vv}, K_{co}\right) + \sin(\theta) \int_{\Delta t} f''\left(\eta_{hh}, \eta_{vv}, \rho_{co}^{vol}\right) \cdot L\left(k_{hh}, k_{vv}, K_{co}\right) dt}{f'\left(\sigma_{SARhh}^{0}, \sigma_{SARvv}^{0}\right)} \tag{2.6}$$

where σ_{xx}^{ground} and ρ_{co}^{ground} are respectively the co-polar backscattering coefficient (at polarization x) and the complex correlation coefficient of the ground target (i.e., the pixel), η_{xx} and ρ_{co}^{vol} the reflectivity (at polarization x) and the complex correlation coefficient of the atmospheric cell, θ is the incident angle and K_{co} is the specific differential phase, accounting for the phase rotation along the incident and backscattered paths. The functions f, f' and f'' in (2.6) are complex functions of the surface and volume scattering matrix elements.

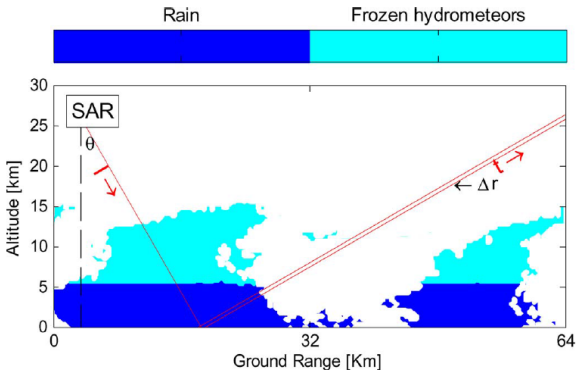

Fig. 2. SAR cross-track observation section. The incident direction is the l coordinate, whilst the wavefront, simplified as planar, is along the t coordinate; Δr is the resolution cell, while θ is the incident angle. The hydrometeor distributions can be roughly schematize as given by a liquid water particle layer (up to freezing level) and a frozen particle one (above).

While target parameters can be derived from SEM/SEAWIND2 simulations, the radiative volume variables η_{xx}, ρ_{co}^{vol}, k_{xx} and K_{co} have to be computed using the SAM particle water content W distributions. In this work we have derived these parameters (generally denoted as p) using power law models of the form $p = a \cdot W^{b}$, where a, b are coefficients derived by HESS T-Matrix simulations for the given incident angle and wavelength and for each model hydrometeor class. Further details are indicated in (Marzano et al., 2012).

3 Results and discussion

In order to evaluate the outcomes of the revised SAR response model, we have compared results with numerical simulations derived from (Marzano et al., 2012) model for the same test case. In order to simplify interpretation of results, we have adopted a homogenous ground target (SEM bare soil) with a 2-layer homogeneous hydrometeor distribution.

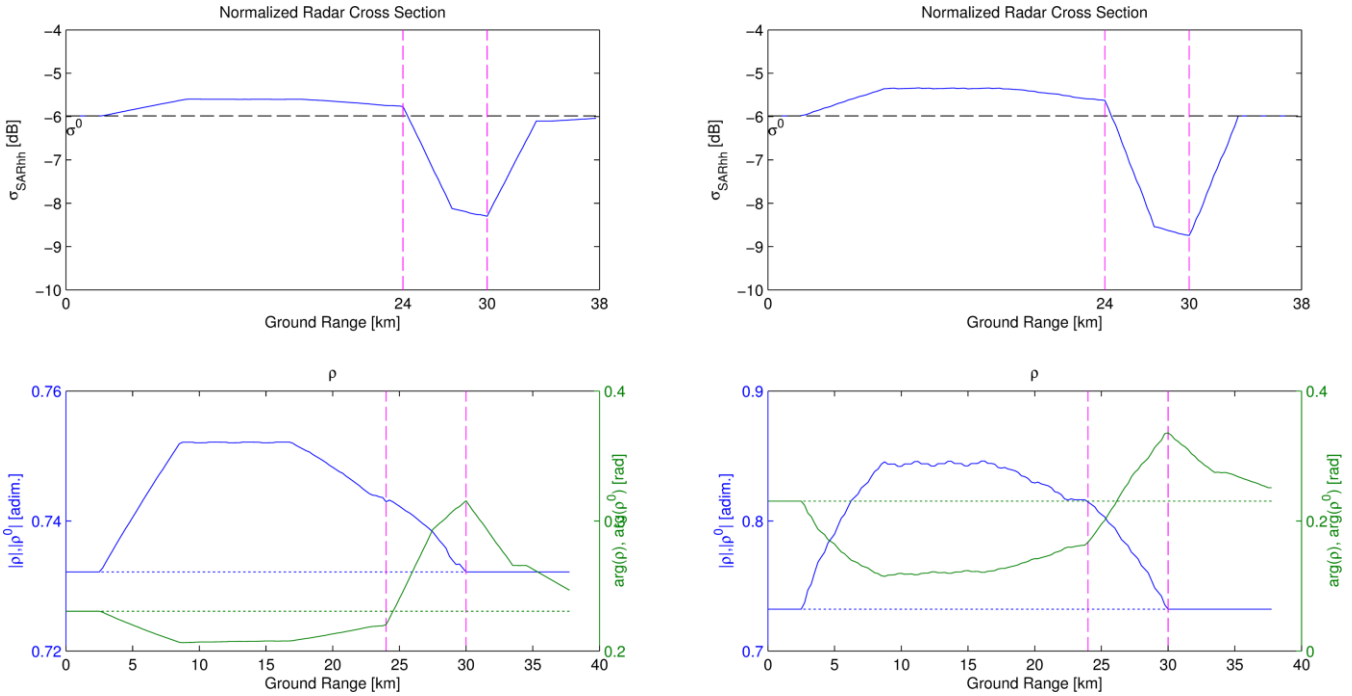

Fig. 3. Comparison at X-Band between the revised SAR response model (left) and the one described in (Marzano et al., 2012) (right) for the basic 2-Layer test case and SEM bare soil homogeneous ground. Top plots show the NRCS [dB] at HH polarization; Bottom plots show module (right ordinate, [adim]) and phase (left ordinate, [rad]) of the simulated complex correlation coefficient. Continuous lines are SAR response; dotted ones are the ground target; cloud boundaries are indicated by magenta vertical lines.

Figure 3 shows results for X-Band. We can observe that NRCS range is more compact in the revised model, with reduced frozen particles enhancements and reduced attenuations, while the overall trend is the same. Similar considerations hold for the complex correlation coefficient also, with reduced variations both in module and argument respect the previous model framework; moreover trends are more linear, as expected, respect previous model response.

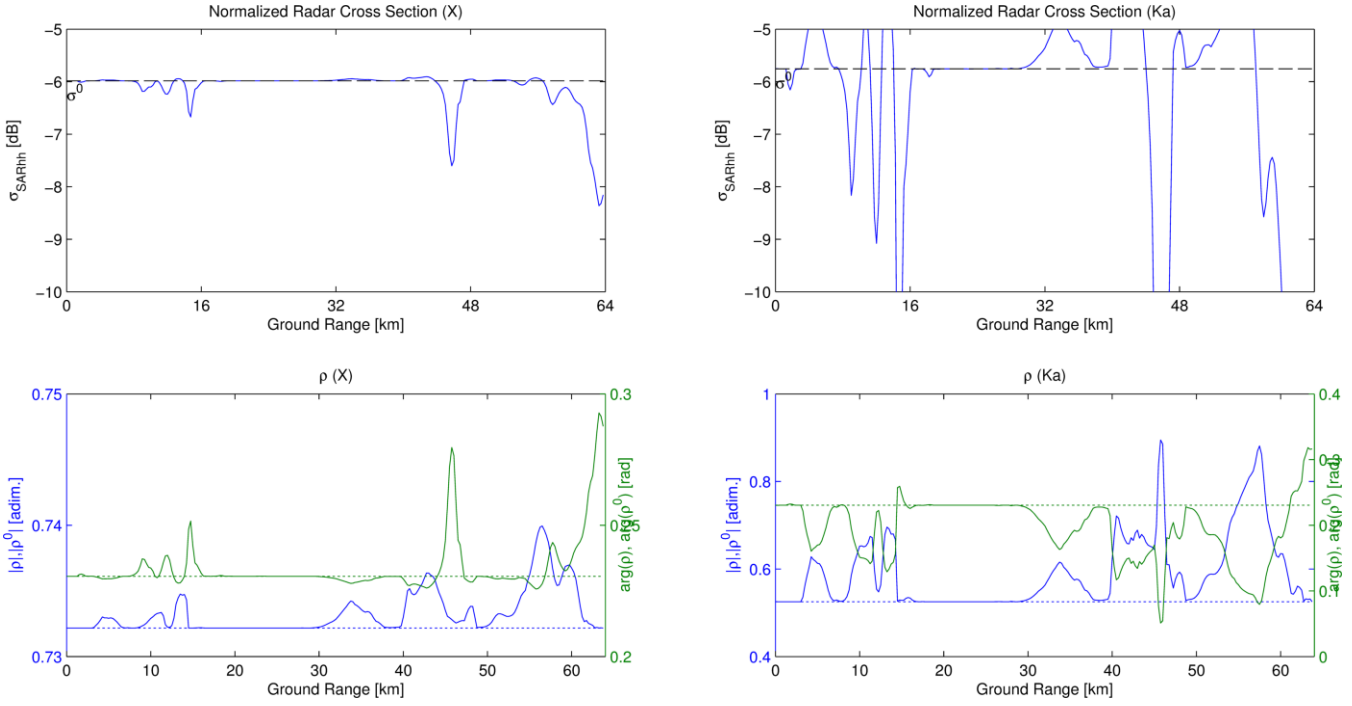

Fig. 4. SAR simulated response for the SAM test case at X-band (Left) and Ka-band (Right) with a SEM bare soil ground surface. Top plots show NRCS at HH polarization [dB] in the same range scale. Bottom plots show module (right ordinate, [adim]) and phase (left ordinate, [rad]) of the complex correlation coefficient. Continuous lines are SAR response; dotted ones are the ground target one.

Modulus of the complex correlation coefficient is determined by the volume contribution, with an initial enhancement respect background, due to frozen particles, and a subsequent reduction down to background value due to reduction of frozen particles and presence of liquid ones. More complex is the analysis of argument. Initially we have a negative shift due to frozen particles within the volume contribution, and then a positive shift due to liquid ones. Positive rotation increases

rapidly when the incident ray matches the hydrometeors distribution, and then reduces to background value when the incident ray exit the precipitating cloud..

Figure 4 and 5 show other SAR simulation examples obtained by SAM atmospheric simulations. Figure 4 compares X and Ka bands (at 9.6 and 35 GHz respectively) at HH polarization for the same SEM bare soil model of Fig. 3. For NRCS it is noted a similar trend between the two bands with a larger sensitivity at Ka-band. A similar behavior is also noted for modulus of complex correlation coefficient, even if differences exist (see for example after km 55). It is worth noticing that while NRCS background response is similar between the two bands, the correlation coefficient background is significantly different between X and Ka band.

Finally, Figure 5 shows a simulation at X-Band HH polarization, using the SAM test case and a marine surface model by SEAWIND2 and SAM wind speeds at 23.7 m AMSL. The analysis is only in terms of NRCS, due to the unavailability of surface complex correlation coefficients in SEAWIND2 output. The larger variability of background echoes is apparent, influencing the spaceborne NRCS; nevertheless atmospheric volume effects are noticeable and lead to an increase of SAR NRCS.

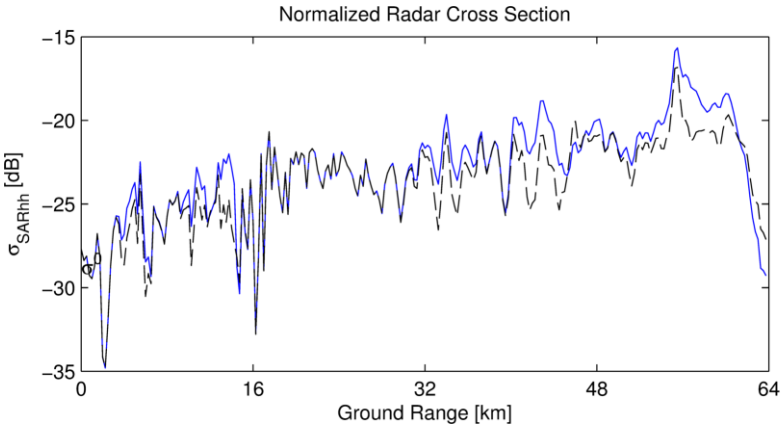

Fig. 5. SAR simulated response NRCS at HH polarization [dB] for the SAM test case at X-band with a SEAWIND2 marine surface and wind speed [m/s] at 23.7 m AMSL derived by SAM dataset. Continuous lines are SAR response; dotted are the ground target one.

4 Conclusions

A revised multiband polarimetric SAR response model for precipitations has been developed. The coupling of an high resolution Cloud Resolving Model (i.e. SAM), ground surface models (i.e. SEM for bare soil and SEAWIND2 for sea surface) and the HESS T-Matrix model for hydrometeors scattering parameterization has allowed us to design an overall polarimetric response model taking into account SAR slant geometry in both amplitude and phase. Indeed, the SAR observation has been treated equivalent to a SLAR one, an approximation which might be realistic since ground resolution is degraded to about 500 m. Same example simulations have been shown for sea and ground surfaces at both X and Ka bands, confirming the greater sensitivity of Ka-band to the presence of a scattering with respect the X-Band, and the importance of wind for sea surface observations. Much work and test cases are required to verify and validate the proposed model, including comparison with independent measurements, such as spaceborne SAR observations, weather radar data or spaceborne radiometer soundings; nevertheless these preliminary results are promising. Together with validation, future work foresees an extension of the sea surface model to include not only wind speed effects but also precipitations ones. The proposed model will be used within the ESA project “Ka-band SAR backscatter analysis in support of future applications” to simulate spaceborne Ka-band SAR response in presence of different kind of precipitating clouds and several basic targets. Finally the proposed SAR forward model will be also used to test new inversion methodologies to be applied to spaceborne SAR precipitation measurements, one of the objectives of the EU project “Earth2Observe”.

Acknowledgement

This work has been partially supported by the European Union’s DG Research FP7 programme within the Earth2Observe “Global Earth Observation for Integrated Water Resource Assessment” project (http://www.earth2observe.eu/) and by ESA within the “Ka-band SAR backscatter analysis in support of future applications” project (ESA/ESTEC contract N. 4000109477/13/nl/lvh.

References

Baldini L. and Roberto, N. and Gorgucci, E. and Fritz, J. and Chandrasekar, V. Analysis of dual polarization images of precipitating clouds collected by the COSMO SkyMed constellation. // Atmospheric Research – 2014.: Vol. 144 – pp. 21–37

Blossey P.N. and Bretherton, C.S. and Cetrone, J. and Khairoutdinov, M. Cloudresolving model simulations of KWAJEX: Model sensitivities and comparisons with satellite and radar observations // J. Atmos. Sci. – 2007.: Vol. 64. - No. 5. - pp. 1488–1508.

Bringi V.N., and Chandrasekar, V. Polarimetric Doppler Weather Radar // Cambridge university press. – 2001.

Covello F. and Battazza, F. and Coletta, A. and Lopinto, E. and Fiorentino, C. and Pietranera, L. and Valentini, G. and Zoffoli, S. COSMO-SkyMed an existing opportunity for observing the Earth // J. Geodyn. – 2010.: Vol. 49. – pp. 171-180.

Danklmayer A. and Doring, B. and Schwerdt, M. and Chandra, M. Assessment of atmospheric propagation effects in SAR // IEEE Trans. Geosci. Rem. Sensing. - 2009.; Vol. 47. - pp. 3507-3518.

Marzano F.S. and Mori, S. and Weinman, J.A. Evidence of Rainfall Signatures on X-Band Synthetic Aperture Radar Imagery Over Land // IEEE Trans. Geosci. Rem. Sens. - 2010.: Vol. 48. – No. 2. - pp. 950-964.

Marzano F.S. and Mori, S. and Chini, M. and Pulvirenti, L. and Pierdicca, N. and Montopoli, M. and Weinman, J.A. Potential of high-resolution detection and retrieval of precipitation fields from X-band spaceborne synthetic aperture radar over land // Hydrology and Earth System Sciences. - 2011.: Vol. 15. - pp. 859-875.

Marzano F.S. and Mori, S. and Montopoli, M. and Weinman, J.A. Modeling Polarimetric Response of Spaceborne Synthetic Aperture Radar due to Precipitating Clouds from X to Ka band // IEEE Trans. Geosci. Rem. Sens. - 2012.: Vol. 50. – No. 3. – pp. 687-703.

Oh Y. and Sarabandi, K. and Ulaby, F.T. Semi-empirical model of the ensemble-averaged differential Muller matrix for microwave backscattering from bare soil surfaces // IEEE Trans. Geosci. Remote Sens.- 2002.: Vol. 40. - No. 6. - pp. 1348–1355.

Pierdicca N. and Pulvirenti, L. Comparing Scatterometric and Radiometric Simulations With Geophysical Model Functions to Tune a Sea Wave Spectrum Model // IEEE Trans. Geosci. Rem. Sensing. – 2008.: Vol. 46. - No. 11. - pp. 3756 - 3767.

Pulvirenti L. and Marzano, F.S. and Pierdicca, N. and Mori, S. and Chini, M. Discrimination of water surfaces, heavy rainfall and wet snow using COSMO-SkyMed observations of severe weather events // IEEE Trans. Geosci. Rem. Sensing. – 2014.: Vol. 52. – No. 2. – pp. 858 – 869.

Ulaby F.T., and Elachi, C. Radar Polarimetry for Geoscience Applications // Artech house. – 1990.

Weinman J.A. and Marzano, F.S. An exploratory study to derive rainfall over land from spaceborne synthetic aperture radars // J. Appl. Meteor. Climate, - 2008.: Vol. 47. - No. 2. - pp. 562–575.

Werninghaus R. and Buckreuss, S. The TerraSAR-X Mission and System Design // IEEE Trans. Geosci. Rem. Sensing. – 2010.: Vol. 48. – pp. 606-614.